Del Campo, R., Savoini, B., Jordao, L., Muñoz, A., & Monge, M. A. (2017). Cytocompatibility, biofilm assembly and corrosion behavior of mg-HAP composites processed by extrusion. *Materials Science and Engineering: C,* 78, 667-673

DOI: https://doi.org/10.1016/j.msec.2017.04.143

Cytocompatibility, biofilm assembly and corrosion behavior of Mg-HAP composites processed by extrusion

R. Del Campo[a, *], B. Savoini[a, b], L. Jordao[c], A. Muñoz[a, b], M.A. Monge[a, b]

[a] *Universidad Carlos III de Madrid, Departamento de Física, Avda. de la Universidad 30, 28911 Leganés, Spain*
[b] *Instituto Tecnológico de Química y Materiales Alvaro Alonso Barba (IAAB), Avda. Universidad 30, 28911 Leganés, Spain*
[c] *Instituto Nacional de Saúde Dr. Ricardo Jorge, Departamento de Saúde Ambiental, Avenida Padre Cruz, 1649-016 Lisboa, Portugal*

Article history:
Received 2 September 2016
Received in revised form 18 April 2017
Accepted 22 April 2017
Available online xxx

A B S T R A C T

In this work the cytocompatibility of pure magnesium and Mg-xHAP composites (x = 5, 10 and 15 wt%) fabricated by powder metallurgy routes has been investigated. The materials were produced from raw HAP powders with particle mean sizes of 6 μm (S-xHAP) or 25 μm (L-xHAP). The biocompatibility study has been performed for MC3T3 cells (osteoblasts/osteoclasts) and L929 fibroblasts. The results indicate that S-Mg (pure magnesium), S-10HAP and L-10HAP composites are the materials with the best biocompatibility. The ability of *S. aureus* bacteria to assemble biofilms was also evaluated. Biofilm formation assays showed that these materials are not particular prone to colonization and biofilm assembly is strain dependent. The corrosion resistance of S-Mg, S-10HAP and L-10HAP materials immersed in the media used for the cells culture has also been analyzed. Different trends in the corrosion resistance have been found: S-Mg and S-10HAP show a very high resistance to corrosion whereas the corrosion of L-10HAP steadily increases with time.

1. Introduction

Surgical steel and cobalt and titanium-based materials are widely used in the bio-medical field, in particular in orthopedic applications. However, the use of these materials implies certain risks [1–3] as the introduction of toxic elements into the biological system due to the materials corrosion and the appearance of stress shielding events associated to the mismatch of the mechanical properties between the metal implant and the osseous tissues. Besides, once the tissue has healed, in some cases a secondary surgery for the implant removal is required.

In the last decades, lot of research has been performed on biodegradable materials with medical applications [4,5]. The goal is to obtain materials susceptible to be used as temporary implants, for which a second surgery is not necessary and no material is left in the body that could lead to possible inflammation or long-term allergic reactions. Additionally, post-operative implant-related bacterial infections are the most common complications after surgery, which may cause a significant danger to patients [6]. The initial attachment of bacteria to the implant surface may lead to bacterial colonization, biofilm formation and implant-related bacterial infection [7,8].

Pure Mg and Mg-based compounds have a great potential as temporary biomaterials for implants applications [9–12]. Pure Mg is a very light material, with a density of 1.74 g/cm^3, which is 1.6 and 4.5 times lower than those of aluminum and steel, respectively [13]. The elastic modulus and compressive yield strength of Mg are very close to those of the natural bone, what reduces the appearance of stress shielding effects. Furthermore, magnesium is present in the human body, so it exhibits a very high biocompatibility. Although magnesium has a low corrosion resistance in aqueous environments, the corrosion products are not toxic for the human body and can harmlessly be eliminated in the urine [14]. However, the magnesium corrosion implies the degradation of the mechanical properties of the implant, what is dangerous if the tissue is not sufficiently healed [15]. Furthermore, in the corrosion process, hydrogen gas is released at a very high rate originating a significant accumulation of gas that will diffuse through the tissues but that could not be properly eliminated [13,16]. In a certain way, these drawbacks can be mitigated by alloying magnesium with other elements that must also exhibit a high biocompatibility [4,9] or modifying the implant surface, for instance by passivation, oxidation or coating deposition [10,17,18].

In this work, magnesium-hydroxyapatite (Mg-HAP) composites with different HAP contents and HAP characteristics have been produced by extrusion. Synthetic HAP has an excellent similarity to the inorganic component of the bone matrix [19]. Due to its excellent bioactivity and osteoconductive properties it can act like nucleation points for the new bone [20–30]. Some studies show that ceramic materials, like hydroxyapatite (HAP), alter the frequency or extent of bacterial colonization [31–37]. Recently, the mechanical properties and the corrosion resistance in a phosphate buffered saline (PBS) solution of some of these composites were investigated [38]. However, it is essential to carry out in vitro experiments in order to study the cytotoxicity of the corrosion products. As the potential applications

* Corresponding author.
Email address: rcampo@fis.uc3m.es (R. Del Campo)

for these new materials are in the field of bone regeneration, the study has been realized with osteoblasts and fibroblasts line cells [39]. Additionally the ability of the *Staphylococcus aureus* bacteria to form biofilms has been investigated, as these bacteria account for a high percentage of orthopedic implant infections [8].

2. Experimental procedure

2.1. Materials

Pure magnesium and Mg-HAP composites were fabricated following two powder metallurgy routes. The starting powders were magnesium with a purity of 99.8% and a particle mean size of 38 μm (Alfa Aesar), and hydroxyapatite with two particle mean sizes: 25 μm (BABI-HAP-P; Berkeley Advanced Biomaterials) and 6 μm (P220 S; Plasma Biotal Limited).

Mg powder was mixed with the BABI-HAP-P powder at ratios of 100:0, 95:5, 90:10 and 85:15 wt% in a turbula mixer during 6 h and compacted in silicone moulds by cold isostatic pressing under a 250 MPa pressure. Cylindrical bars of these compacts, denoted as L-xHAP (x = 0, 5, 10 and 15) were produced by conventional extrusion in air at 400 °C and 2 mm/s speed with a section reduction ratio of 11.

Mg and P220 S hydroxyapatite powder, with the same series of weight ratios, were also mixed and compacted. Cylindrical bars, labeled as S-xHAP (x = 0, 5, 10 and 15) were consolidated by extrusion at 400 °C, at a speed of 0.5 mm/s and a section reduction ratio of 10.

Disc samples were cut from the bars, grinded with abrasive SiC papers and polished with α-Al_2O_3 (0.3 μm particle size). The samples were cleaned with absolute ethanol in an ultrasonic bath for several minutes, sterilized with UV light for 24 h and kept in a vacuum environment.

2.2. Cells and culture media

Mouse bone calvaria MC3T3-E1 cells (ATCC CRL-2593) and mouse subcutaneous connective tissue L929 cells (ATCC CCL-1) were used to assay the osteoblast and fibroblast cell response, respectively. MC3T3-E1 cells were cultured in α-MEM medium (Life technologies) supplemented with 10 vol% of fetal bovine serum (FBS-Lonza), 100 UI/ml penicillin and streptomycin (Difco). L929 cells were cultured in RPMI-1640 medium (Lonza) containing 10% FBS (v/v), 100 UI/ml penicillin, 100 UI/ml streptomycin, 2 mM L-glutamine (Difco) and 1 mM sodium pyruvate (Difco). Cells were subcultured according to the supplier's instructions using 0.25%/0.02% (v/v) trypsin/EDTA solution (Gibco) and kept at 37 °C with an atmosphere of 5% carbon dioxide.

Osteoblast differentiation into osteoclasts was achieved after 10 days incubation at 37 °C/5% CO_2 in α-MEM medium supplemented with 50 μg/ml L-ascorbic acid (Sigma) and 3.0 mM inorganic phosphate (total concentration of inorganic phosphate 3.5 mM) as described previously [40]. Additionally Alizarin red staining (Sigma) was performed according to manufactures instructions to confirm the matrix mineralization characteristic of differentiation into osteoclasts.

2.3. Bacteria and culture media

Two methicillin resistant *S. aureus* strains were used in this work: a reference strain ATCC 12600 T (MRSA-1) and a clinical isolate (MRSA-2). Fresh overnight cultures were grown on Mueller-Hinton agar (Oxoid) for the biofilm assays.

2.4. Test methods

2.4.1. Extracts preparation

The extracts were prepared according to EN ISO 10993. Briefly, samples of all materials were incubated for 24 h at 37 °C/5% CO_2 in cell culture media in a surface to volume ratio of 1.25 cm^2 per ml. The resulted extracts were filtered using 0.2 μm cellulose acetate filters (VWR international) and further diluted with cell culture media to 50, 25 and 12.5% concentrations (v/v).

2.4.2. Cytotoxicity assay

Osteoblasts or fibroblasts at a cell density of 6000 cells per well were seeded in a 96-well-plate (Nunc/Thermo Fisher scientific) and incubated for 24 h at 37 °C/5% CO_2. For the assays with osteoclasts, 600 osteoblasts were seeded per well and incubated at 37 °C/5% CO_2 for 10 days. After 1 day (osteoblasts and fibroblasts) or 10 days (osteoclasts) the cell culture media was replaced by fresh cell culture media (for be used as control) or the different concentrations of magnesium extracts. Further, the cells were incubated for 24 h before assessing the cytotoxic effect of the extracts using MTT assay. Briefly, a 5 mg/ml MTT (Sigma) in PBS solution was tenfold diluted in cell culture media, added to each well and incubated for 4 h at 37 °C/5% CO_2. At this point the MTT solution was removed and the formazan product was dissolved in dimethyl sulfoxide during 15 min at room temperature protected from light. The viability of the cells was quantified by measuring the absorbance at λ = 570 nm in a spectrophotometer. The resulting value for the control (cells incubated with cell culture media) was considered as 100% viability. Cell viability in the extracts was expressed as a percentage of the control viability. According to the EN ISO 10993, if the relative metabolic viability of each type of cell in a medium containing extracts was lower than 70%, the medium was considered as cytotoxic.

2.4.3. Cell morphology

The cytocompatibility tests were extended by performing a study on the proliferation and morphology of the MC3T3 cells. MC3T3 cells at a density of 30,000 cells per well were seeded on glass coverslips inside a 24-well-plate and incubated at 37 °C/5% CO_2 for 24 h. The cell cultures were replaced by the extracts and cultivated for additional 24 h in the same conditions. Cells were fixed with p-formaldehyde (4%) in phosphate buffer saline solution (PBS) for 15 min at room temperature, washed with PBS and incubated for 15 min in 50 mM ammonium chloride before being permeabilized with 0.1% triton X-100 in PBS for 30 min. After blocking for 30 min at room temperature with 0.4% cold water skin fish gelatin in PBS (Sigma), cells were incubated with alexa 568 phalloidin (Molecular probes/Thermo Fisher scientific) diluted 1:50 in blocking solution. After washing with PBS and water, cells were incubated in 5 μg/ml DAPI for 3 min, further washed with water and mounted with fluorescent mounting media (Dabco). Confocal microscopy images were acquired using a Leica Sp2 microscope.

Osteoblasts were seeded on material samples (~ 170 mm^2) within 24 well plates (Nunc) for 24 h at 37 °C/5% CO_2. Cells were fixed with 2.5% glutaraldehyde (EMS), 4% p-formaldehyde (Sigma) for 2 h at room temperature. This was followed by post-fixation in the dark with 1% osmium tetroxide (EMS), and then washed twice with PBS and water, dehydrated, transferred to glass slides (bioMérieux) and dried at room temperature. Samples were mounted on a sample holder with carbon tape, sputter-coated with carbon (20 nm) using a Sputter Coater QISOT ES (Quorum Technologies) and analyzed with a scanning electron microscope, JSM-7100F (JEOL).

2.4.4. Biofilm assay

The assay was performed in duplicate using 24-well flat-bottomed cell culture plates (Nunc). Briefly, bacterial suspensions at a final concentration of 10^7 (CFU)/ml were prepared in 0.9% sodium chloride from overnight cultures in Mueller Hinton (MH) agar and ten-fold diluted in osteoclast culture media without antibiotics. Along with a disc of each material, one millilitre of bacterial suspension was distributed per well. The osteoclast culture media was used as the negative control. The plates were incubated at 37 °C to allow biofilm formation for 24 h. The well content was removed, and each well was vigorously washed three times with sterile distilled water. The attached bacteria were stained for 15 min with 600 µl violet crystal at room temperature, washed with distilled water three times and allowed to dry at room temperature. The violet crystal was dissolved in 95% ethanol (Merck), and the optical density at 570 nm was measured using a SpectraMax 340PC apparatus (Molecular Devices). Results were normalized taking into account the area of the discs.

2.4.5. Corrosion measurements

The corrosion behavior in the media used for the cell culture was studied for the specimens that exhibited the best biocompatibility, i.e. S-Mg, L-10HAP and S-10HAP composites. The corrosion rate was measured by collecting the hydrogen released from the reaction of the medium with the Mg. The experimental procedure was described in reference [41]. Cylindrical samples were pasted at the bottom of a 100 ml beaker containing 90 ml of medium. The hydrogen gas was collected by a funnel connected to the burette and the gas volume was registered versus time. The experiments were conducted at 37 °C during 48 h and the sample surface exposed to the corrosion environment was ~ 170 mm^2. Simultaneously, another sample immersed in a similar medium under the same conditions was used to measure the pH evolution.

2.4.6. Statistical analysis

At least six replicates for each condition were done in cytocompatibility tests. All the values were expressed as the mean value ± standard deviation. Statistical significance was assessed by the Student *t*-test (two-tailed) with $p < 0.05$ being considered statistically significant. Regarding the corrosion measurements, for each material three samples were tested.

3. Results and discussion

3.1. Cytocompatibility analysis

Cytotoxicity induced by the products resulted from the materials degradation was tested by evaluating the cellular response of MC3T3 cells in two differentiation stages (osteoblasts and osteoclasts) and L929 cells (fibroblasts), as recommended by EN ISO 10993.

The cytotoxicity results for MC3T3 osteoblast cells challenged with different concentrations of material extracts are shown in Fig. 1 for the S-xHAP and L-xHAP materials. For 100% extracts concentrations, only osteoblast toxicity was observed for L-Mg, S-5HAP and S-15HAP extracts. Moreover, for extracts contents ≤ 50% no cytoxicity effect was observed for any material.

In contrast, the relative metabolic viability for the fibroblast cells L929 is below 70% for all the materials when the extracts content in the medium is 100%, as it is shown in Fig. 2. The toxicity decreases on increasing the extracts dilution and only when the extracts content is below 25% all media are non-cytotoxic.

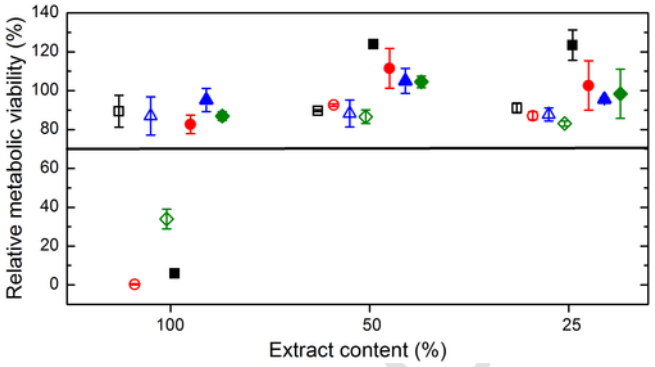

Fig. 1. Metabolic viability of the osteoblast cells versus extract dilutions. Open symbols correspond to S-xHAP samples and filled symbols to L-xHAP samples. S-Mg (□); S-5HAP (○); S-10HAP (Δ); S-15HAP (◊); L-Mg (■); L-5HAP (●); L-10HAP (▲); L-15HAP (♦).

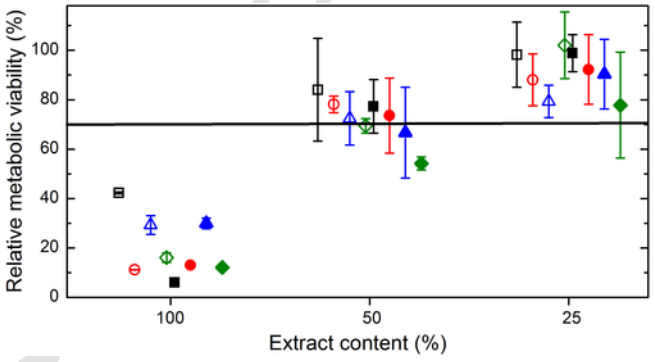

Fig. 2. Metabolic viability of the fibroblast cells versus extract dilutions. Open symbols correspond to S-xHAP samples and filled symbols to L-xHAP samples. S-Mg (□); S-5HAP (○); S-10HAP (Δ); S-15HAP (◊); L-Mg (■); L-5HAP (●); L-10HAP (▲); L-15HAP (♦).

The results for both osteoblast and fibroblast assays indicate that the three materials whose undiluted extracts present the best metabolic viability are S-Mg, S-10HAP and L-10HAP. To complete the characterization of the osteoblast cell line, the viability of osteoclast cells immersed into the undiluted and diluted extracts of these three selected materials was also evaluated. At 100% extracts concentration the viability of osteoclasts is above 70% for the three materials, as is depicted in Fig. 3, where a comparison of the viability values for osteoblasts and osteoclasts is shown. It is noted that for S-Mg and S-10HAP materials the osteoclast viability is higher than the osteoblast one, and increases with the extract dilution.

3.2. Cell adhesion and morphology

Cell morphology was assessed either by confocal microscopy for the osteoblast grown on glass coverslips immersed in undiluted extracts or by SEM for osteoblast grown on the materials. The first experimental approach allowed us to evaluate the cell morphology, cell density, the status of cell nucleus and cytoskeleton. As it is shown in Fig. 4 (a) for S-10HAP composite, both the cell nucleus and cytoskeletons do not exhibit alterations. This fact together with the cell density is in good agreement with the biocompatibility test results. In other words the cells were incubated within a biocompatible media. In contrast, when the osteoblasts were incubated within extracts responsible for biocompatibility rates lower than 70%, a notorious cell density decrease is observed together with cell morphology alter-

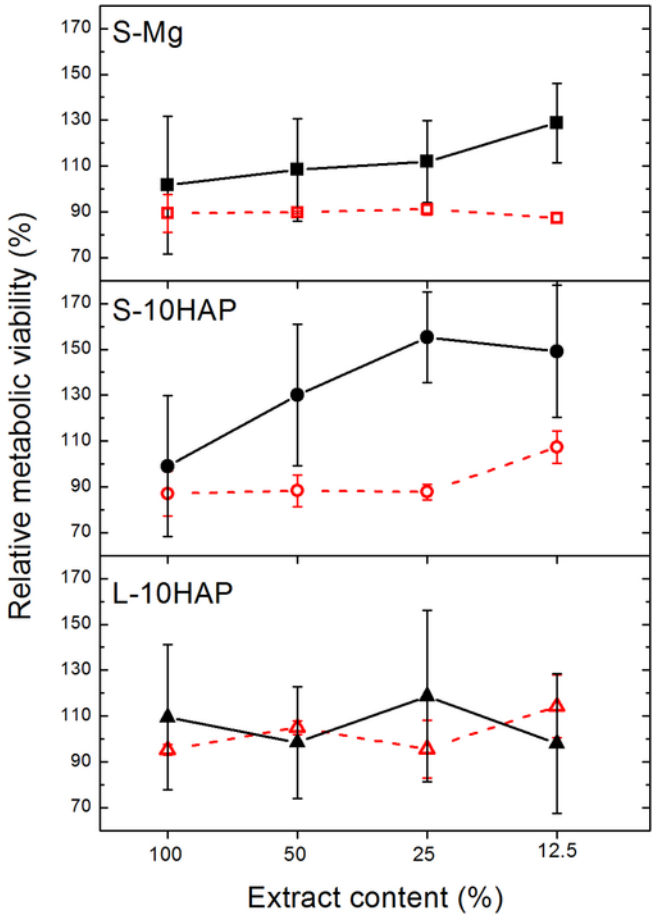

Fig. 3. Metabolic viability of osteoclast (solid symbols) and osteoblast (open symbols) cells versus extract dilution from S-Mg, S-10HAP and L-10HAP samples.

ations, as displayed in Fig. 4 (b) for the S-5HAP composite. To evaluate the ability of osteoblasts to adhere and proliferate on the materials surface, they were grown on the materials and observed by FE-SEM. A representative image of an osteoblast adherent to a S-10HAP sample is shown in Fig. 5. It has to be noted that during the dehydration process the material layer evolved from the corrosion products suffers a contraction, what gives place to some cracks on the matrix that result in the rupture of some cells.

3.3. Biofilm assembly

Meticillin resistant *S. aureus* (MRSA) colonization of orthopedic devices could cause infections difficult to treat. For this reason we evaluated the ability of two MRSA strains to colonize the materials with the best cytocompatibility profiles (S-Mg, S-10HAP and L-10HAP) through a biofilm assembly assay. The results obtained for the negative control, see Fig. 6, indicate that MRSA-1 is significantly a better biofilm assembler than MRSA-2 ($p = 0.0009$). This scenario was reversed for biofilms assembled on S-Mg, S-10HAP and L-10HAP, where MRSA-2 was a better biofilm assembler, although statistically the difference was not significant ($p = 0.07$).

For each material no substantial differences between the biofilm assemblies for the 2 strains were found ($p \geq 0.016$). No differences between the MRSA-1 ability for assembling biofilms on the control and the material surfaces were found, however for the MRSA-2 strain a significant difference between the control and S-Mg and L-10HAP ($p = 0.016$) was found.

These results indicate that biofilm assembly is strain dependent and, for the present assayed strains, S-10HAP is less prone to biofilm colonization by MRSA.

3.4. Corrosion resistance

Corrosion tests for S-Mg, S-10HAP and L-10HAP composites have been carried out by immersing the samples in the cell culture media for 48 h. The volume rate of H_2 released during the corrosion was converted to an average corrosion penetration rate, given in mm/year, following the procedure described in reference [41]. The results are depicted in Fig. 7.

Two different trends in the evolution of the corrosion rate can be observed. Whereas the corrosion rate in all the media steadily increases for L-10HAP, for S-Mg and S-10HAP samples it undergoes a

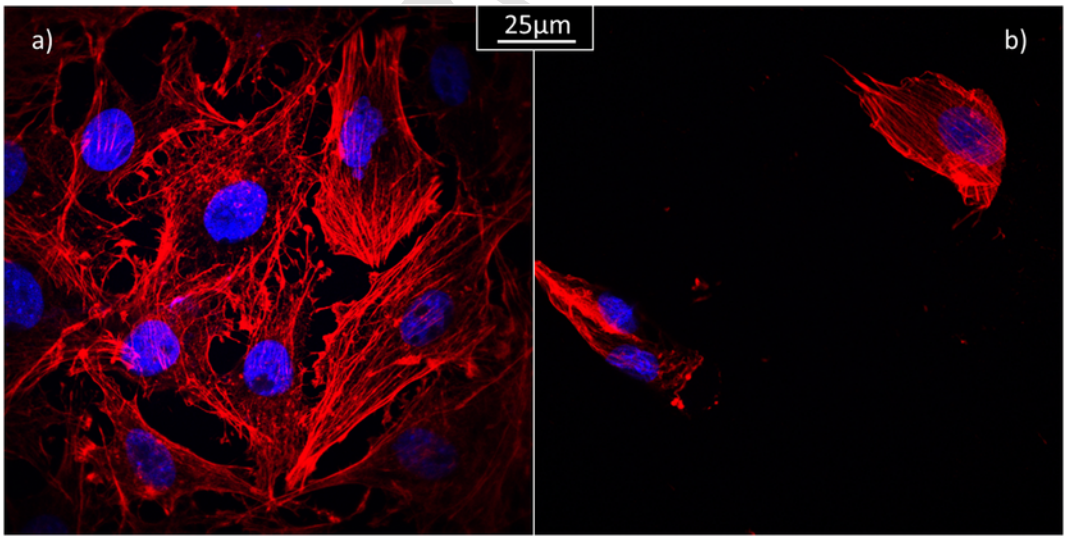

Fig. 4. Confocal Microscopy Images of the osteoblast cells for (a) S-10HAP with no toxicity (b) S-5HAP with a high toxicity, showing the nuclei (blue) and the actin (red). (For interpretation of the references to color in this figure legend, the reader is referred to the web version of this article.)

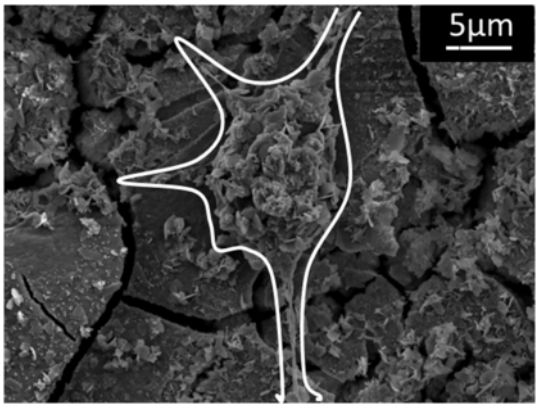

Fig. 5. FE-SEM image of a MC3T3 osteoblast cell fixed on the S-10HAP surface.

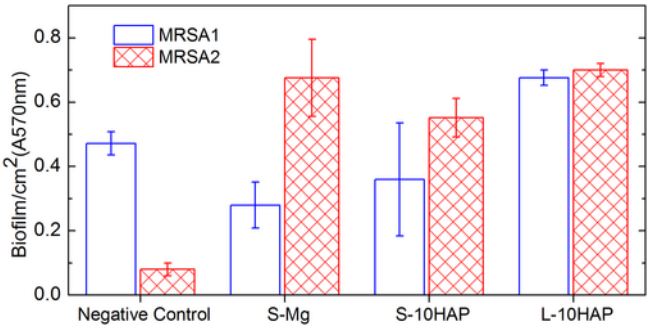

Fig. 6. Biofilm assembly for the two MRSA strains.

sharp decrease in the first 5 h and remains constant at a very low value after 20 h. It indicates that S-Mg and S-10HAP present a very high resistance to corrosion. Moreover, from these curves it can be inferred that the S-10HAP composite presents the highest resistance to the corrosion in the osteoblast medium and S-Mg exhibits the highest resistance to corrosion in the fibroblast medium.

The evolution of the pH medium with the immersion time is shown in Fig. 8. At the initial states, the pH increases at the same rate regardless the material and cell medium, but after that, the pH of the media with S-Mg and S-10HAP materials increases more slowly, reaching values of ~ 8.5 for the osteoclast cell medium and ~ 8.8 for the osteoblast and fibroblast cell media after 48 h. It is noteworthy that, for these materials, the evolution of the pH follows similar trends. On contrary, the pH in the media containing L-10HAP increases up to values around 9.3.

The corrosion of magnesium in aqueous solutions proceeds with the formation of a $Mg(OH)_2$ film on the surface of the magnesium sample. This layer has a protective effect, but its physical integrity is affected by several factors, as the presence of chloride ions that can transforms $Mg(OH)_2$ to the more soluble $MgCl_2$, promoting the sample dissolution. Cell culture media are complex corrosive environments as proteins, dissolved oxygen, and electrolyte ions can contribute as inhibitors or accelerators of the Mg dissolution. Has been reported in a number of studies the formation and precipitation of several compounds like Mg- and Ca-containing phosphates that act as passive layers on the sample surface and improve the corrosion resistance of the composite. This resistance depends on the layer-forming characteristics (i.e., solubility, density, porosity) [42–44]. In such a way, at the initial states the Mg dissolution leads to a strong increase of the pH value, but the subsequent formation of the protective films in the alkaline solutions radically reduces the corrosion rate and slows down the increase of the pH value, as Figs. 7 and 8 reveal.

The metabolic activity of MC3T3-E1 and L929 cells may be directly influenced by the released ions from the sample, or by increased pH-values. Several studies have shown the relationship between magnesium and bone formation and the effects of different concentrations of magnesium on bone cells, positively associating the osteoblast viability with the concentration of Mg ions and the duration of exposure. This effect was observed for concentrations lower than 10 mM [45,46]. However the tolerance level depends on the tested cell line.

On the other hand, the presence of Mg^{2+} and the corrosion products along with the increase of the pH could have an effect on the *S. aureus* bacteria growth and the formation of biofilms. It has been re-

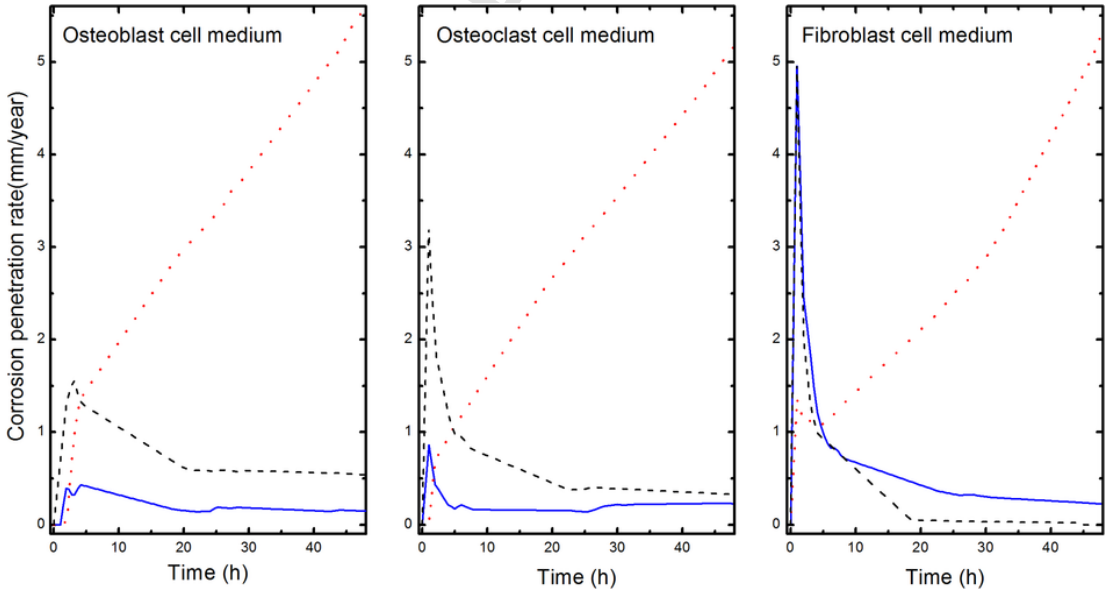

Fig. 7. Corrosion penetration rate in the culture media as a function of time for S-Mg (dashed line), S-10HAP (solid line) and L-10HAP (dotted line).

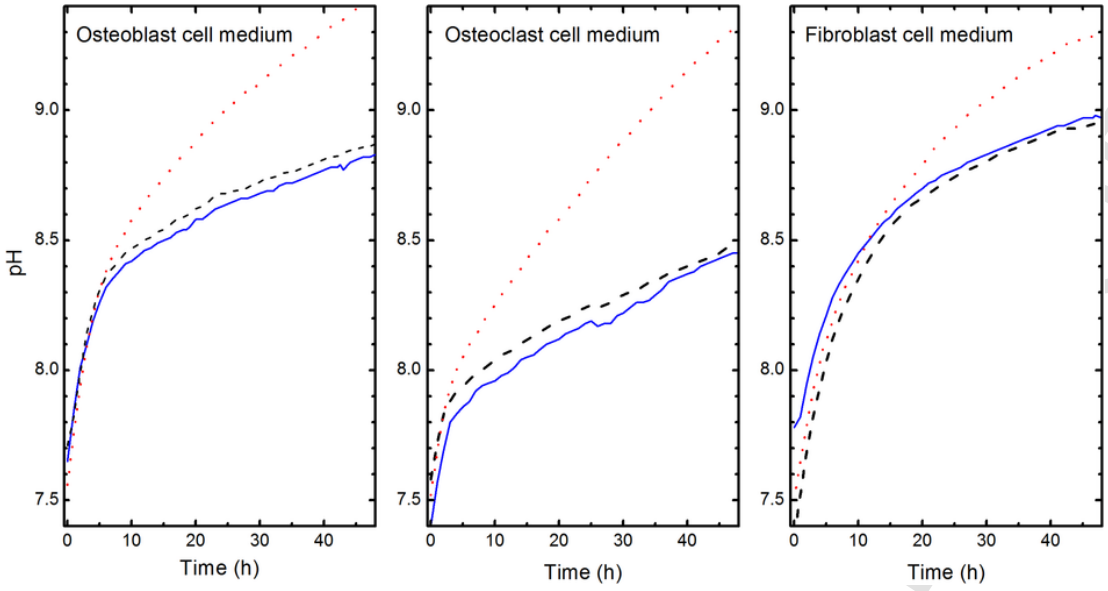

Fig. 8. Evolution of the solutions pH with the immersion time for S-Mg (dashed line), S-10HAP (solid line) and L-10HAP (dotted line).

ported that an increase of the alkalinity (i.e. higher pH) would inhibit bacterial growth [47] and that Mg^{2+} and Ca^{2+} may be membrane-active and bactericidal agents against *S. aureus* [48]. The formation of a biofilm is a complex process involving an initial attachment and a subsequent maturation phase which are physiologically different from each other. Furthermore, the mechanisms of biofilm formation and the ability to form fully established biofilms may be different for diverse strains of the same bacteria specie [8]. The adhesion step is highly dependent on the properties of the material surface on which the biofilm is developing, as the topography and the roughness. Several studies have reported the bacterial response to nano/microstructured surfaces, but the results are not conclusive [49,50]. The microstructure of S-Mg, S-10HAP and L-10HAP consist of elongated grains with a length ranging from 30 to 40 μm and widths from 2.5 to 5 μm. Although there are no significant variations in the grain size among the three materials, HAP is found forming agglomerates within the matrix with sizes range from 2 to 50 μm in the case of L-10HAP sample and from 0.1 to 6 μm for S-10HAP sample [38]. In this last sample the HAP is also present decorating the grain boundaries. These features could affect to the adhesion of the bacterial cells. In addition, due to the Mg corrosion and the formation of non-stable protective layers, the surface topography of the materials is constantly changing. As the dissolution rate is higher for the L-10HAP sample, this effect on the bacterial adherence was expected to be stronger, as Fig.6 shows.

4. Conclusions

This work demonstrates that powder metallurgical composites of Mg-HAP with HAP content up to 15 wt%, produced from raw HAP powders with particle mean sizes of 6 μm (S-HAP) or 25 μm (L-HAP), have no toxic effects on the viability of MC3T3 cells (osteoblasts/osteoclasts) and L929 fibroblasts at dilutions ≥ 50%. At 100% extracts concentration the three materials that present the best metabolic viability are S-Mg, S-10HAP and L-10HAP, with viability higher than 70% for the osteoblast/osteoclast lines. The degradation resistance of these materials immersed in the cell culture media is much higher for S-Mg and S-10HAP than for L-10HAP. Analyses of the ability to form biofilms of two strains of the *S. aureus* bacteria show that these materials are not particular prone to be colonized. The results indicate that biofilm assembly is strain dependent and, for the present assayed strains, S-10HAP is less prone to biofilm colonization by *S. aureus*.

Acknowledgements

This work has been supported by the Regional Government of Madrid through the S2013/MIT-2862-MULTIMAT-CHALLENGE Program. R del Campo thanks to the Universidad Carlos III de Madrid for the support.

References

[1] Q. Chen, G.A. Thouas, Metallic implant biomaterials, review, Mater. Sci. Eng. R 87 (2015) 1–57.
[2] S. Kulanthaivel, B. Roy, T. Agarwal, S. Giri, K. Pramanik, K. Pal, S.S. Ray, T.K. Maiti, I. Banerjee, Cobalt doped proangiogenic hydroxyapatite for bone tissue engineering application, Mater. Sci. Eng. C 58 (2016) 648–658.
[3] J. Nagels, M. Stokdijk, P.M. Rozing, Stress shielding and bone resorption in shoulder arthroplasty, J. Shoulder Elb. Surg. 12 (2003) 35–39.
[4] Y.F. Zheng, X.N. Gu, F. Witte, Biodegradable metals, review, Mater. Sci. Eng. R 77 (2014) 1–34.
[5] J. Yan, Y. Miao, H. Tan, T. Zhou, Z. Ling, Y. Chen, X. Xing, X. Hu, Injectable alginate/hydroxyapatite gel scaffold combined with gelatin microspheres for drug delivery and bone tissue engineering, Mater. Sci. Eng. C 63 (2016) 274–284.
[6] R.O. Darouiche, Treatment of infections associated with surgical implants, N. Engl. J. Med. 350 (2004) 1422–1429.
[7] J.W. Costerton, Biofilm theory can guide the treatment of device-related orthopaedic infections, Clin. Orthop. Relat. Res. 437 (2005) 7–11.
[8] K. Smith, A. Perez, G. Ramage, D. Lappin, C.G. Gemmell, S. Lang, Biofilm formation by Scottish clinical isolates of Staphylococcus aureus, J. Med. Microbiol. 57 (2008) 1018–1023.
[9] X.N. Gu, Y.F. Zheng, A review on magnesium alloys as biodegradable materials, Front Mater. Sci. China 4 (2010) 111–115.
[10] S.V. Dorozhkin, Calcium orthophosphate coatings on magnesium and its biodegradable Alloys, review, Acta Biomater. 10 (2014) 2919–2934.
[11] S. Agarwal, J. Curtin, B. Duffy, S. Jaiswal, Biodegradable magnesium alloys for orthopaedic applications: a review on corrosion, biocompatibility and surface modifications, Mater. Sci. Eng. C 68 (2016) 948–963.
[12] K.F. Farraro, K.E. Kim, S.L.Y. Woo, J.R. Flowers, M.B. Mccullough, Revolutionizing orthopaedic biomaterials: the potential of biodegradable and bioresorbable magnesium-based materials for functional tissue engineering, J. Biomech. 47 (2014) 1979–1986.

[13] M.P. Staiger, A.M. Pietak, J. Huadmai, G. Dias, Magnesium and its alloys as orthopedic biomaterials: a review, Biomaterials 27 (2006) 1728–1734.

[14] J. Vormann, Magnesium: nutrition and metabolism, Mol. Asp. Med. 24 (2003) 27–37.

[15] Y. Jang, Z. Tan, C. Jurey, Z. Xu, Z. Dong, B. Collins, Y. Yun, J. Sankar, Understanding corrosion behavior of Mg-Zn-Ca alloys from subcutaneous mouse model: effect of Zn element concentration and plasma electrolytic oxidation, Mater. Sci. Eng. C 48 (2015) 28–40.

[16] F. Witte, V. Kaese, H. Haferkamp, E. Switzer, A. Meyer-Lindenberg, C.J. Wirth, H. Windhagen, In vivo corrosion of four magnesium alloys and the associated bone response, Biomaterials 26 (2005) 3557–3563.

[17] T. Hanawa, In vivo metallic biomaterials and surface modification, Mater. Sci. Eng. A 267 (1999) 260–266.

[18] P. Roach, D. Eglin, K. Rohde, C.C. Perry, Modern biomaterials: a review—bulk properties and implications of surface modifications, J. Mater. Sci. Mater. Med. 18 (2007) 1263–1277.

[19] V.P. Orlovskii, V.S. Komlev, S.M. Barinov, Hydroxyapatite and hydroxyapatite-based ceramics, Inorg. Mater. 38 (2002) 973–984.

[20] A. Pietak, P. Mahoney, G.J. Dias, M.P. Staiger, Bone-like matrix formation on magnesium and magnesium alloys, J. Mater. Sci: Mater. Md. 19 (2008) 407–415.

[21] K.P. Ananth, A.J. Nathanael, S.P. Jose, T.H. Oh, D. Mangalaraj, A novel silica nanotube reinforced ionic incorporated hydroxyapatite composite coating on polypyrrole coated 316L SS for implant application, Mater. Sci. Eng. C 59 (2016) 1110–1124.

[22] C. Sharma, A.K. Dinda, P.D. Potdar, C.F. Chou, N.C. Mishra, Fabrication and characterization of novel nano-biocomposite scaffold of chitosan-gelatin-alginate-hydroxyapatite for bone tissue engineering, Mater. Sci. Eng. C 64 (2016) 416–427.

[23] A. Atila, Z. Halici, E. Cadirci, E. Karakus, S.S. Palabiyik, N. Ay, F. Bakan, S. Yilmaz, Study of the boron levels in serum after implantation of different ratios nano-hexagonal boron nitride-hydroxy apatite in rat femurs, Mater. Sci. Eng. C 58 (2016) 1082–1089.

[24] D. Loca, M. Sokolova, J. Locs, A. Smirnova, Z. Irbe, Calicum phosphate bone cements for local vancomycin delivery, Mater. Sci. Eng. C 49 (2015) 106–113.

[25] A. Belcarz, J. Zalewska, K. Palka, M. Hajnos, G. Ginalska, Do Ca^{2+}-adsorbing ceramics reduce of calcium ions from gypsum-based biomaterials?, Mater. Sci. Eng. C 47 (2015) 256–265.

[26] H. Esfahani, M.P. Prabhakaran, E. Salahi, A. Tayebifard, M.R. Rahimipour, M. Keyanpour-Rad, S. Ramakrishna, Electrospun nylon 6/zinc doped hydroxyapatite membrane for protein separation: mechanism of fouling and blocking model, Mater. Sci. Eng. C 59 (2016) 420–428.

[27] G. Radha, S. Balakumar, B. Venkatesan, E. Vellaichamy, Evaluation of hemocompatibility and in vitro immersion on microwave-assisted hydroxyapatite-alumina nanocomposites, Mater. Sci. Eng. C 50 (2015) 143–150.

[28] M.K. Sah, S.N. Rath, Soluble eggshell membrane: a natural protein to improve the properties of biomaterials used for tissue engineering applications, Mater. Sci. Eng. C 67 (2016) 807–821.

[29] O. Kaygili, S. Keser, M. Kom, Y. Eroksuz, S.V. Dorozhkin, T. Ates, I.H. Ozercan, C. Tatar, F. Yakuphanoglu, Strontium substituted hydroxyapatites: synthesis and determination of their structural properties, in vitro and in vivo performance, Mater. Sci. Eng. C 55 (2015) 538–546.

[30] T. Koshino, T. Murase, T. Takagi, T. Saito, New bone formation around porous hydroxyapatite wedge implanted in opening wedge high tibial osteotomy in patients with osteoarthritis, Biomaterials 22 (2001) 1579–1582.

[31] C. Arciola, L. Montanaro, A. Moroni, M. Giordano, A. PIezzoferrato, M. Donati, Hydroxyapatite coated orthopaedic screws as infection resistant materials, in vitro study, Biomaterials 20 (1999) 323–327.

[32] N. Ignjatovic, V. Wu, Z. Ajdukovic, T. Mihajilov-Krstev, V. Uskokovic, D. Uskokovic, Chitosan-PLGA polymer blends as coatings for hydroxyapatite nanoparticles and their effect on antimicrobial properties, osteoconductivity and regeneration of osseous tissues, Mater. Sci. Eng. C 60 (2016) 357–364.

[33] U. Hess, G. Mikolajczyk, L. Treccani, P. Streckbein, C. Heiss, S. Odenbach, K. Rezwan, Multi-loaded ceramic beads/matrix scaffolds obtained by combining ionotropic and freeze gelation for sustained and tuneable vancomycin release, Mater. Sci. Eng. C 67 (2016) 542–553.

[34] E. Zeimaran, S. Pourshahrestani, I. Djordjevic, B. Pingguan-Murphy, N.A. Kadri, M.R. Towler, Bioactive glass reinforced elastomer composites for skeletal regeneration: a review, Mater. Sci. Eng. C 53 (2015) 175–188.

[35] R.K. Singh, S. Awasthi, A. Dhayalan, J.M.F. Ferreira, S. Kannan, Deposition, structure, physical and in vitro characteristics of Ag-doped β-$Ca_3(PO_4)_2$/chitosan hybrid composite coatings on Titanium metal, Mater. Sci. Eng. C 62 (2016) 692–701.

[36] S.M. Romanelli, K.R. Fath, A.P. Phekoo, G.A. Knoll, I.A. Banerjee, Layer-by-layer assembly of peptide based bioorganic-inorganic hybrid scaffolds and their interactions with osteoblastic MC3T3-E1 cells, Mater. Sci. Eng. C 51 (2015) 316–328.

[37] S. Jegatheeswaran, S. Selvam, V.S. Ramkumar, M. Sundrarajan, Novel strategy for f-Hap/PVP/Ag nanocomposite synthesis from fluoro based ionic liquid assistance: systematic investigations on its antibacterial and cytotoxicity behaviors, Mater. Sci. Eng. C 67 (2016) 8–19.

[38] R. del Campo, B. Savoini, A. Muñoz, M.A. Monge, G. Garcés, Mechanical properties and corrosion behavior of Mg-HAP composites, J. Mech. Behav. Biomed. Mater. 39 (2014) 238–246.

[39] M. Saqaei, M. Fathi, H. Edris, V. Mortazavi, Preparation and biocompatibility evaluation of bioactive glass-forsterite nanocomposite powder for oral bone defects treatment applications, Mater. Sci. Eng. C 56 (2015) 409–416.

[40] D. Wang, K. Christensen, K. Chawla, G. Xiao, P.H. Krebsbach, R.T. Franceschi, Isolation and characterization of MC3T3-E1 preosteoblast subclones with distinct in vitro and in vivo differentiation/mineralization potential, J. Bone Miner. Res. 14 (6) (1999) 893–903.

[41] Z. Shi, A. Atrens, An innovative specimen configuration for the study of Mg corrosion, Corros. Sci. 53 (2011) 226–246.

[42] H. Altun, S. Sen, Studies on the influence of chloride ion concentration and pH on the corrosion and electrochemical behaviour of AZ63 magnesium alloy, Mater. Design 25 (2004) 637–643.

[43] S. Hiromoto, T. Shishido, A. Yamamoto, N. Maruyama, H. Somekawa, T. Mukai, Precipitation control of calcium phosphate on pure magnesium by anodization, Corros. Sci. 50 (2008) 2906–2913.

[44] H.X. Wang, S.K. Guan, X. Wang, C.X. Ren, L.G. Wang, In vitro degradation and mechanical integrity of Mg–Zn–Ca alloy coated with Ca-deficient hydroxyapatite by the pulse electrodeposition process, Acta Biomater. 6 (2010) 1743–1748.

[45] C. Yang, G. Yuan, J. Zhang, Z. Tang, X. Zhang, K. Dai, Effects of magnesium alloys extracts on adult human bone marrow derived stromal cell viability and osteogenic differentiation, Biomed. Mater. 5 (2010) 045005–045014.

[46] L.Y. He, X.M. Zhang, B. Liu, Y. Tian, W.H. Ma, Effect of magnesium ion on human osteoblast activity, Braz. J. Med. Biol. Res. 49 (7) (2016) 1–7.

[47] D.A. Robinson, R.W. Griffith, D. Shechtman, R.B. Evans, M.G. Conzemius, In vitro antibacterial properties of magnesium metal against Escherichia coli, Pseudomonas aeruginosa and Staphylococcus aureus, Acta Biomater. 6 (2010) 1869–1877.

[48] Y. Xie, L. Yang, Calcium and magnesium ions are membrane-active against stationary-phase Staphylococcus aureus with high specificity, Sci. Report. 6 (2016) 20628–20636.

[49] K. Anselme, P. Davidson, A.M. Popa, M. Giazzon, M. Liley, L. Ploux, The interaction of cells and bacteria with surfaces structured at the nanometre scale, Acta Biomater. 6 (2010) 3824–3846.

[50] K. Bohinca, G. Dražić, A. Abram, M. Jevšnik, B. Jeršek, D. Nipič, M. Kurinčič, P. Raspo, Metal surface characteristics dictate bacterial adhesion capacity, Int. J. Adhes. Adhes. 68 (2016) 39–46.